The PSIG procedure to Persistent Scatterer Interferometry (PSI) using X-band and C-band Sentinel-1 data

María Cuevas-González*[a], Núria Devanthéry[a], Michele Crosetto[a], Oriol Monserrat[a], Bruno Crippa[b]
[a]Geomatics Division, Centre Tecnològic de Telecomunicacions de Catalunya (CTTC), Av. Gauss 7, E-08860, Castelldefels (Barcelona), Spain; [b]Department of Earth Sciences, University of Milan, Via Cicognara 7, I-20129, Milan, Italy

ABSTRACT

A new approach to Persistent Scatterer Interferometry (PSI) data processing and analysis implemented in the PSI chain of the Geomatics (PSIG) Division of CTTC is used in this work. The flexibility of the PSIG procedure allowed evaluating two different processing chains of the PSIG procedure. A full PSIG procedure was implemented in the TerraSAR-X dataset while a reduced PSIG procedure was applied to the nine Sentinel-1 images available at the time of processing. The performance of the PSIG procedure is illustrated using X-band and C-band Sentinel-1 data and several examples of deformation maps covering different types of deformation phenomena are shown.

Keywords: PSI, C-band, X-band, Sentinel-1, Terrasar-X, deformation measurement

1. INTRODUCTION

Satellite-based radar interferometric techniques allow measuring and monitoring a wide range of deformation phenomena (Hanssen, 2001; Crosetto et al., 2010) such as subsidence, slope instability, landslides, or deformation in urban areas. The Persistent Scatterer Interferometry (PSI) technique (Ferreti et al., 2000) is based on the use of a stack of images acquired by a satellite over a given area at different times.

The PSI technique is ideally suited to measure the spatial extent and magnitude of surface deformation due to its wide spatial coverage and millimetre precision. In fact, it allows obtaining a comprehensive outlook of the deformation phenomena occurring in wide areas while, at the same time, maintaining the capability to measure individual features such as buildings or infrastructures.

However, there are some limitations of the PSI technique worth mentioning: 1) the PSI technique relies on coherence and, therefore, is opportunistic, which means that it is only able to estimate deformation over the available Persistent Scatterers (PSs), i.e. those points where PSI phases maintain good quality over time to get reliable deformation estimates; 2) PSI suffers limitations in its capability to measure "fast" deformation phenomena due to the ambiguous nature of PSI observations, which are 2π-wrapped. Although it is difficult to quantify what "fast" means, in the case of TerraSAR-X data, movements of up to 0.77 cm of displacement in 11 days between pairs of Persistent Scatterers (PSs) can be measured; 3) the spatial sampling is variable and, as the availability of PSs depends on coherence, in urban areas the sampling will probably be reasonably good but PSI tends to fail in vegetated and forested areas. Besides, PS locations are not known before processing; and 4) the deformation measurements are made in the direction of the Line-Of-Sight (LOS) of the satellite.

The launch of X-band sensors such as TerraSAR-X and CosmoSkyMed represented an improvement compared to previous C-band SAR satellite images. The main advantage of the X-band data resides in its higher spatial resolution (Adam et a., 2008; Crosetto et al., 2010) which leads to a dense PS sampling. Besides, the quality of both the residual topographic error (RTE) and the PS geocoding is very high (Crosetto et al., 2010). The importance of the RTE is two-fold since it plays a key role in the accurate modelling of the PSI observations (i.e. the PSI phases), and also in the geocoding. The magnitude of the topographic phase component of the PSI phase is usually reduced by simulating a synthetic topographic phase using a Digital Elevation Model (DEM) of the observed scene. However, any difference between the true height of a PS and the DEM height generates the so-called residual topographic phase component, which has to be properly modelled, estimated, and separated from the PSI deformation phase component. Additionally, the estimated RTE is used to get an improved geocoding of the PSI products. In this regard, the geocoding location

SAR Image Analysis, Modeling, and Techniques XV, edited by Claudia Notarnicola, Simonetta Paloscia, Nazzareno Pierdicca, Proc. of SPIE Vol. 9642, 96420I
 · doi: 10.1117/12.2194984

errors can be largely reduced and more precise geocoding achieved by using the estimated RTE. X-band observations also show high sensitivity to small displacements related to thermal expansion (Crosetto et al., 2008). Although these effect had already been reported in some studies with C-band PSI (Ferretti et al., 2005; Perissin and Rocca, 2006; Crosetto et al., 2008), they mainly referred to single PSs. In X-band however, the thermal expansion is evident over large sets of PSs enabling the analysis and interpretation of the thermal expansion signal of structures such as buildings and bridges (Monserrat et al., 2011; Crosetto et al., 2015). Therefore, these thermal expansion effects have to be carefully considered in all PSI analysis, especially those covering short observation periods in order to avoid introducing strong distortions in the PSI deformation products, since the thermal expansion in mixed within the total observed displacement. One strategy commonly used nowadays is to explicitly model and estimate the thermal expansion, thus generating a thermal map (Gernhardt et al. 2010; Monserrat et al., 2011; Fornaro et al., 2013; Crosetto et al., 2015), which can be separated from the displacement component.

A further significant improvement in PSI processing is expected due to the data acquisition performance of the C-band sensor onboard the Sentinel-1 satellite. Despite all the advantages of X-band data is important to note than the spatial coverage of TerraSAR-X scenes is approximately 45x45 km, while with the new generation of C-band data sensors as Sentinel-1 a spatial coverage of 250x165km is accomplished. This coverage might be essential for certain applications that might benefit from a wide-area PSI monitoring using C-band Sentinel-1 data. Besides, performing a PSI analysis which requires a large dataset of images is expensive with TerraSAR-X data while Sentinel-1 data is freely available.

A new approach to PSI data processing and analysis implemented in the PSI chain of the Geomatics (PSIG) Division of CTTC is used in this work (Devanthéry et al., 2014). The performance of the PSIG procedure will be illustrated using X-band and C-band Sentinel-1 data and several examples of deformation maps covering different types of deformation phenomena will be shown.

2. METHODOLOGY

2.1 TerraSAR-X PSIG processing

The PSI data processing and analysis were carried out using the PSIG approach described in Devanthéry et al. (2014) and are based on 42 StripMap TerraSAR-X SAR images that cover the period from December 2007 to June 2012. The images are uniformly distributed over the observation period and the perpendicular baselines range from -333 to +506 m.

A stack of N co-registered SAR images, the amplitude dispersion (DA) and M wrapped interferograms, with M>>N, are the main inputs of the PSIG. The PSIG chain is composed of three main processing blocks. In the first block, correctly unwrapped and temporally ordered phases are derived for Persistent Scatterers (PSs) that homogeneously cover the area of interest. In fact, a set of Cousin PSs (CPSs), which are PSs characterized by a moderate spatial phase variation that ensures a correct phase unwrapping, are exploited. Flexible tools are employed in this block to check the consistency of phase unwrapping and guarantee a uniform CPS coverage. The second block is dedicated to estimate the atmospheric phase screen (APS) by exploiting the phases estimated in the first block. Finally, the deformation velocity and time series of deformation of the selected CPSs are derived in the third block. A new 2+1D phase unwrapping algorithm is exploited in this final stage of the PSIG procedure.

The main PSIG processing steps (Fig. 1) are as follows: (1) Candidate Cousin PS (CPS) selection. A set of PSs with phases characterized by a moderate spatial variation is sought in this step, in which at least a seed PS is required to initiate a search for its “cousins”, i.e. PSs with similar characteristics; (2) 2D phase unwrapping. 2D phase unwrapping is performed on the candidate CPSs using a redundant set of M interferograms; (3) Phase unwrapping consistency check. This check is based on a least squares estimation followed by the analysis of the so-called residuals. The final set of CPSs is selected at this stage; (4) APS estimation and removal. The APS is estimated using the selected CPSs and subsequently removed from the original interferograms, thus obtaining a set of M APS-free interferograms; (5) Estimation of deformation velocity and residual topographic error (RTE). The M wrapped APS-free interferograms are used to estimate the deformation velocity and RTE over a dense set of PSs (much denser than the selected CPSs) using the method of the periodogram. Optionally, an extension of the two-parameter model can be used to account for the thermal expansion; (6) RTE removal. The RTE phase component is removed from the wrapped APS-free interferograms.

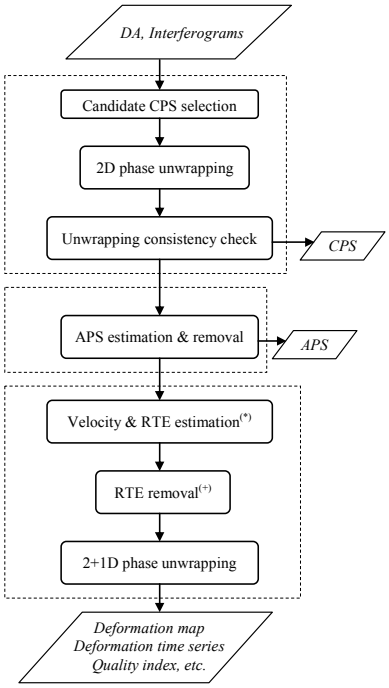

Figure 1. Flow chart showing the main processing steps of the PSIG chain. The dashed lines indicate the three main processing blocks. The full PSIG chain was used to process the TerraSAR-X data while the simplified version was employed in the processing of the Sentinel-1 data.

The linear deformation component can optionally also be removed and then, in a later stage, added back to the deformation time series. The same procedure can be applied to the thermal expansion component; and (7) 2+1D phase unwrapping. A 2+1D phase unwrapping is performed on the set of M APS- and RTE-free interferograms in order to obtain the final deformation phase time series, a quality index for each time series and other parameters related to the detection and correction of unwrapping errors.

2.2 Sentinel-1 processing

Nine Interferometric Wide swath (IW) Single Look Complex (SLC) Sentinel-1 images covering the period from March to May 2015 were used in this study. The spatial resolution of these images is approximately 3 x 20 km in range and azimuth, respectively. The processing was performed burst-wise over the multi-looked interferograms (1 in azimuth and 5 in range). The deformation phases were retrieved directly from the interferometric phases of the eight consecutive temporally connected interferograms over a set of points selected using a temporal consistency criterion (PTCs). The interferograms used have a temporal baseline of 12 days and perpendicular baselines ranging between -104 and 110 m.
The steps performed to derive the deformation measurements are: (1) Pixel selection using a temporal consistency of the interferometric phases. The selection criterion is based on an index computed point wise over all the combinations of interferometric triplets; i.e. all the possible combinations of each existing triplet of images. The index is calculated and normalized as follows:

$$\gamma = \frac{1}{N}\sum_{1}^{N} e^{i(\varphi_{ij}+\varphi_{jk}-\varphi_{ik})}$$

where N is the number of phase combinations found in the network and φ_{ij}, φ_{jk}, φ_{ik} are the interferometric phases calculated from the images *i*, *j*, *k*. It can be demonstrated that the higher the noise of the multi-looked point the lower the index is; in this case a threshold of 0.98 has been used; (2) APS estimation and removal. The APS is estimated using a spatial filter over the above selected PTCs and then removed from the wrapped interferograms; (3) Estimation of the

deformation phase time series. A 2D phase unwrapping is performed using the Minimum Cost Flow method (Costantini, 1998; Costantini et al., 1999) over the eight APS cleaned interferograms and the time series are calculated as follows:

$$\begin{cases} \varphi_j = \varphi_{j-1} + \Delta\varphi_{j(j-1)} \\ \varphi_0 = 0 \end{cases}$$

Where φ_j is the accumulated deformation phase at time j with respect the first acquisition time (φ_0) and $\Delta\varphi_{j(j-1)}$ is the interferometric phase calculated from the images j and j-1.

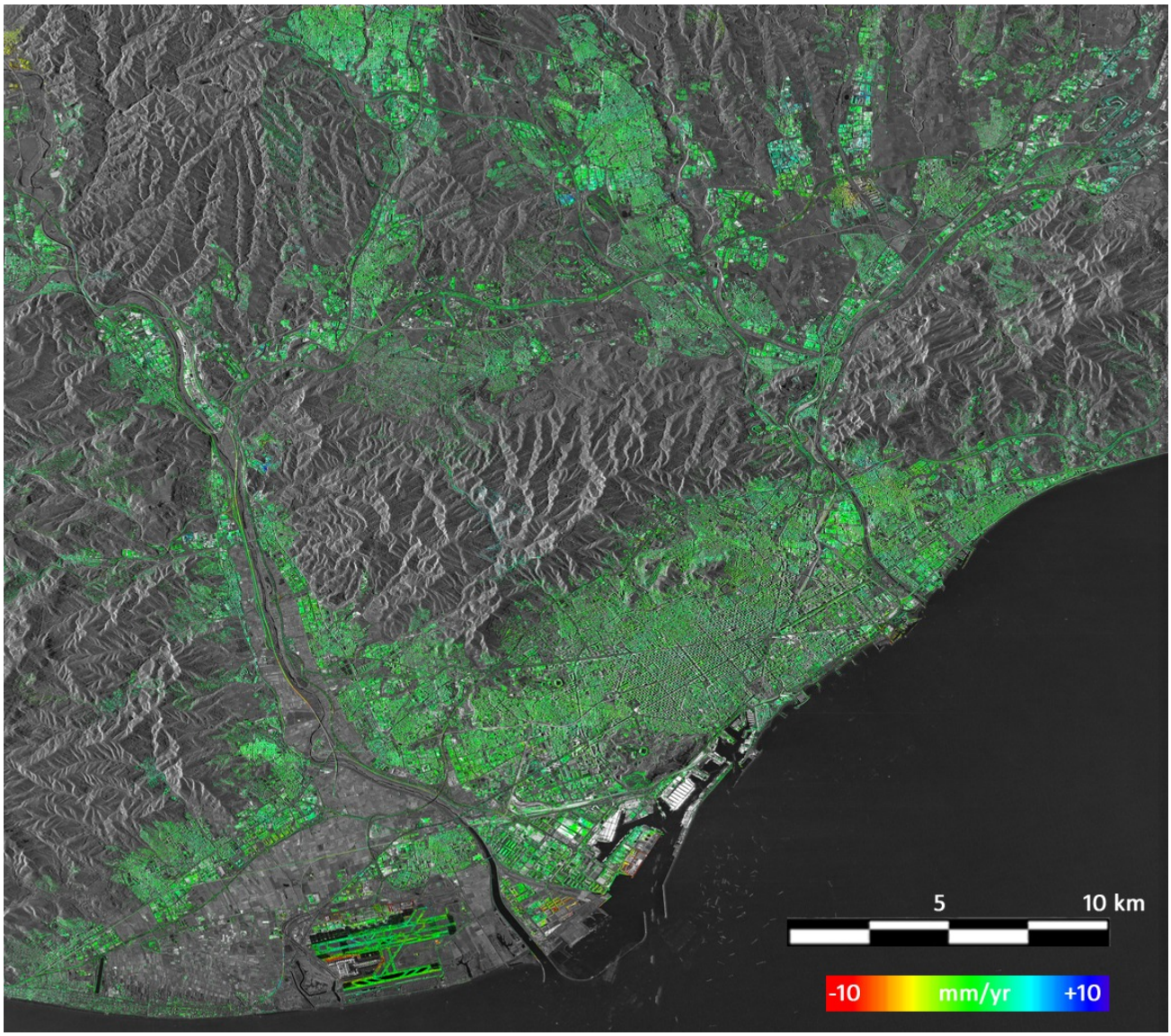

Figure 2. Map of deformation velocity of the Barcelona dataset superimposed over the mean amplitude. This map was derived from 42 TerraSAR-X images spanning the period 2007-2012. The area processed covers 1019 km^2 and over 5.4 million Persistent Scatterers (PSs).

3. RESULTS

The flexibility of the PSIG procedure allowed evaluating two different processing chains of the PSIG procedure. A full PSIG procedure was implemented in the TerraSAR-X dataset while a direct deformation phase retrieval from the interferograms was applied to the nine Sentinel-1 images available at the time of processing.

The TerraSAR-X dataset encompass the metropolitan area of Barcelona and some adjacent towns and countryside areas. The dataset includes 42 images and 633 interferograms (almost the full set of possible interferograms). Figure 2 shows the map of deformation velocity estimated for the entire scene, which comprises more that 5.4 million CPSs and covers and area of 1019 km^2. Positive values (blue) indicate displacements towards the SAR sensor, while negative values (red) denote displacements away from the sensor. It is important to highlight that these values refer to the SAR Line-of-Sight (LOS). Although only the major deformation phenomena, such as those in the airport and port of Barcelona (located at the bottom of the image) and several areas affected by subsidence and uplift (situated at the upper right part of the image), are visible in Fig. 2, additional smaller terrain displacements were found in this scene. These other deformation phenomena include examples of deformation due to soil compaction, water abstraction, landslides, or underground construction works (metro line and metro stations) which represent a valuable source of information.

The Sentinel-1 scene encompasses approximately 50% of the territory of Catalonia (Spain) and a part of the southeast of France and covers approximately 250x167 km divided in three swaths, each containing nine bursts. Since the proposed procedure is implemented burst-wise and, at the time of processing, the results for Catalonia were the priority, the area processed however is smaller, finally including five burst of swath 2 and six bursts of swath 3, accounting for approximately 10500 km^2. The deformation accumulated between March and May 2015 (Fig. 3) was estimated for a

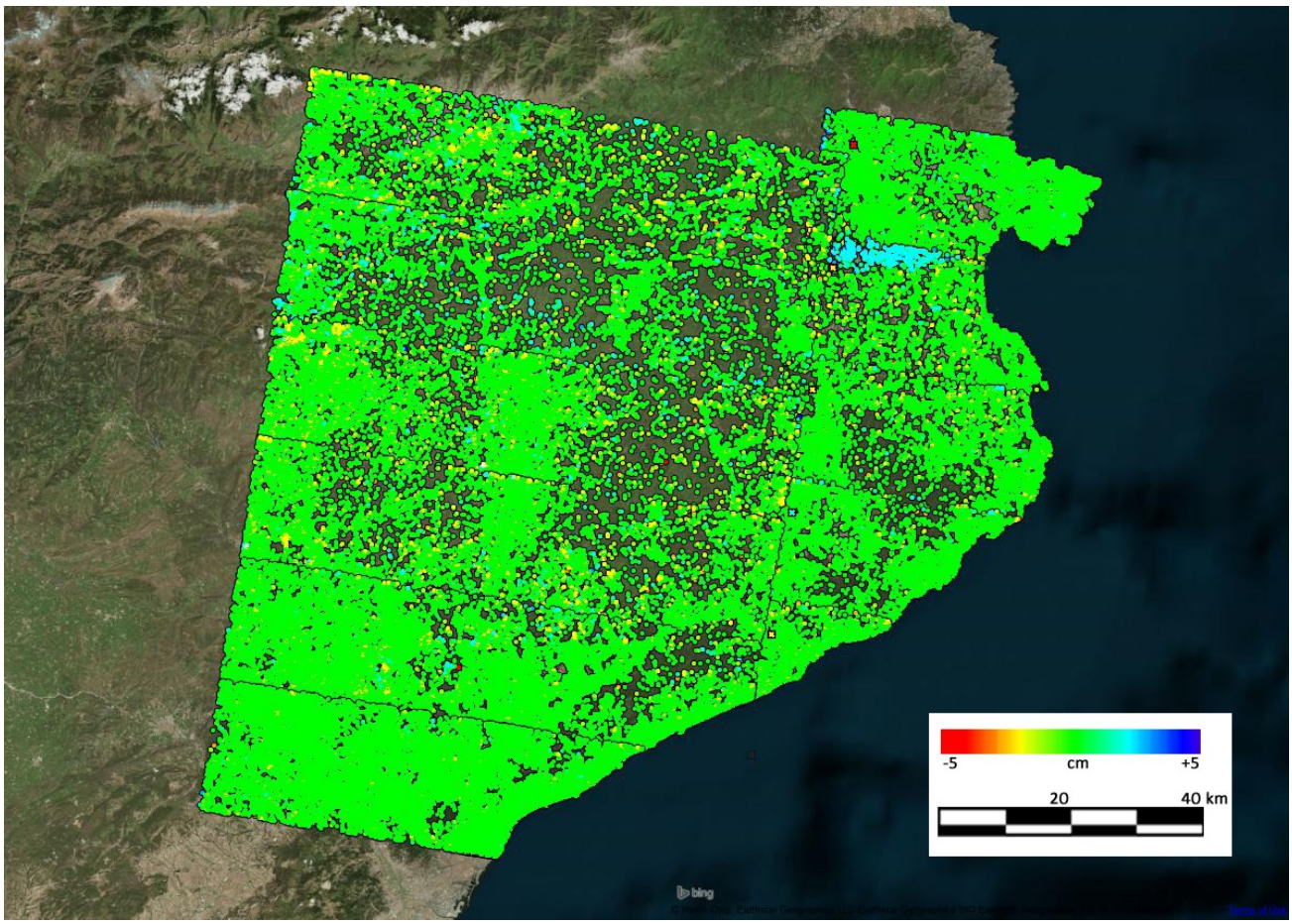

Figure 3. Map of deformation accumulated in the period March to May 2015 estimated from nine Sentinel-1 images.

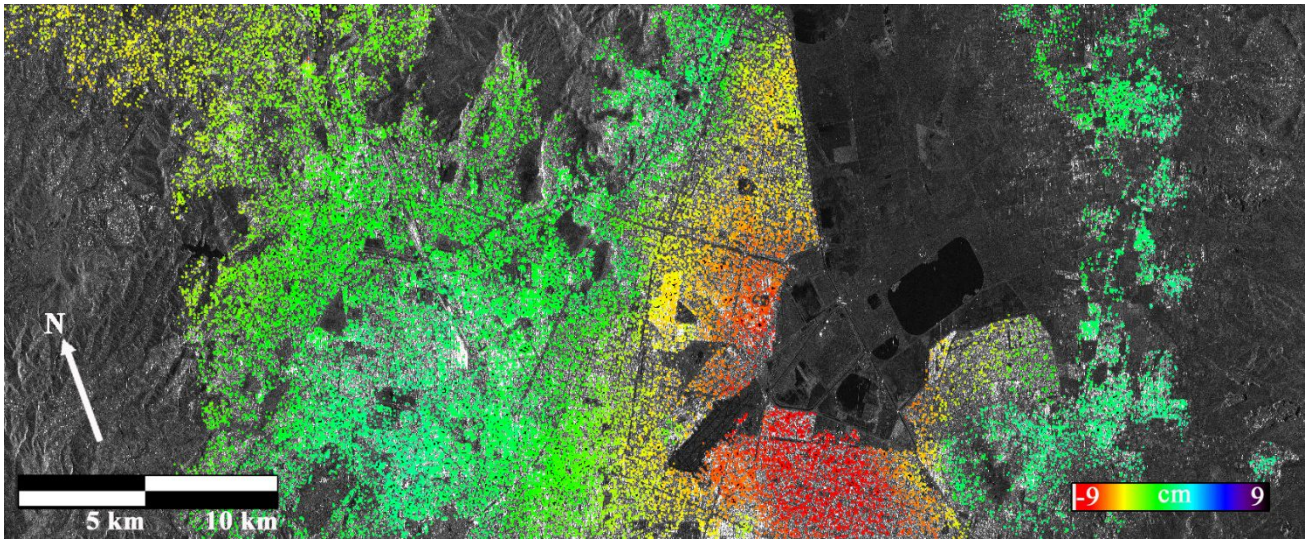

Figure 4. Deformation map of a significant portion of Mexico DF estimated from ten Sentinel-1 images covering the period from October 2014 to January 2015.

total of 417 427 PTCs. As in the case of TerraSAR-X, the estimated deformation refers to the SAR LOS. Note that although the deformation map obtained from Sentinel-1 data are very noisy, these are preliminary results obtained from only nine images, a small dataset for a PSI analysis, which usually requires 15 images or more. Besides, the processing carried out did not involve the estimation of the RTE, which means that the deformation estimated will probably be mixed with the RTE signal. Further work involving a larger dataset and more complex PSIG processing will surely result in an improvement of the estimation. In any case, the density of PSs achieved is promising for certain applications.

This work was originally devoted to compare the results obtained from the PSIG processing of TerraSAR-X and Sentinel-1 data in the area of Catalonia. However, some issues related to the area covered (the frame of the first two images contained a burst that covered the city of Barcelona, which disappeared in subsequent images) and the poor results obtained from Sentinel-1 data encouraged us to show an area processed in a similar manner using a simplified PSIG procedure that resulted in a successful deformation map. Figure 4 shows the deformation map of portion of Mexico DF. The area processed covers approximately 80 x 25 km and a total of 720 882 CPSs were processed. The map shows a large area known to be affected by subsidence (red) with displacement values of up to 9 cm occurred during the four months of observations.

4. CONCLUSIONS

The performance of the PSIG procedure with X- and C-band data has been evaluated in this work. The PSIG processing chain has been applied to two datasets composed of 42 TerraSAR-X images and nine Sentinel-1 images and the results have been shown. The results indicate that the full PSIG chain applied to the TerraSAR-X data performed adequately. In fact, several deformation phenomena, including examples of deformation due to soil compaction, water abstraction, landslides, or underground construction works (metro line and metro stations), were detected. However, the deformation map obtained from Sentinel-1 data is noisy. In this regard, it is essential to point out that this is a preliminary result that might be related to the fact that only nine images were used in the analysis, which represents a small dataset for a PSI analysis that usually requires 15 images or more. Besides, the processing performed on the Sentinel-1 dataset did not involve the estimation of the RTE which could also have an influence in the results. Further work involving a larger dataset and more complex PSIG processing will surely result in an improvement of the estimation. In any case, the density of PTCs achieved is promising for certain applications that require a wide-area deformation monitoring.

ACKNOWLEDGEMENTS

This work has been partially funded by the Spanish Ministry of Economy and Competitiveness through the project MIDES (Ref: CGL2013-43000-P).

REFERENCES

[1] Adam, N., Eineder, M., Yague-Martinez, N., Bamler, R., "High resolution interferometric stacking with TerraSAR-X," Proceedings of IGARSS (2008), Boston, Massachusetts.
[2] M. Costantini, "A novel phase unwrapping method based on network programming," IEEE Transactions on Geoscience and Remote Sensing 36(3), 813–821 (1998).
[3] Costantini, M., Farina, A., Zirilli, F., "A fast phase unwrapping algorithm for SAR interferometry," IEEE Transactions on Geoscience and Remote Sensing 37(1), 452– 460 (1999).
[4] Crosetto, M., Biescas, E., Duro, J., Closa, J., Arnaud, A., "Generation of advanced ERS and Envisat interferometric SAR products using the stable point network technique," Photogrammetric Engineering & Remote Sensing 74(4), 443-450 (2008).
[5] Crosetto, M., Monserrat, O., Iglesias, R., Crippa, B., "Persistent Scatterer Interferometry: potential, limits and initial C- and X-band comparison," Special Issue "High-resolution Earth imaging from geospatial information" of Photogrammetric Engineering and Remote Sensing 76(9), 1061-1069 (2010).
[6] Crosetto, M., Monserrat, O., Cuevas-González, M., Devanthéry, N., Luzi, G., Crippa, B., "Measuring thermal expansion using X-band persistent scatterer interferometry," ISPRS J. 100, 84-91 (2015).
[7] Devanthéry, N., Crosetto, M., Monserrat, O., Cuevas-González, M., Crippa, B., "An approach to Persistent Scatterer Interferometry: the PSIG chain," Remote Sensing 6, 6662-6679 (2014) [doi:10.3390/rs6076662].
[8] Ferretti, A., Perissin, D., Prati, C., Rocca, F., "On the physical nature of SAR Permanent Scatterers," Proceedings of URSI Commission F Symposium on Microwave Remote Sensing of the Earth, Oceans, Ice and Atmosphere, Ispra, Italy (2005).
[9] Ferretti, A., Prati, C., Rocca, F., "Nonlinear subsidence rate estimation using permanent scatterers in differential SAR interferometry", IEEE Transactions on Geoscience and Remote Sensing 38(5), 2202–2212 (2000).
[10] Fornaro, G., Reale, D., Verde, S., "Bridge thermal dilation monitoring with millimeter sensitivity via multidimensional SAR imaging", IEEE Geosci. Remote Sens. Lett. 10, 677–681 (2013).
[11] Gernhardt, S., Adam, N., Eineder, M., Bamler, R., "Potential of very high resolution SAR for persistent scatterer interferometry in urban areas", Annals of GIS 16 (2), 103–111 (2010).
[12] Monserrat, O., Crosetto, M., Cuevas, M., Crippa, B., "The thermal expansion component of Persistent Scatterer Interferometry observations", IEEE Geosci. Remote Sens. Letters 8, 864–868 (2011).
[13] Hanssen, R., [Radar interferometry], Kluwer Academic Publishers, Dordrecht (The Netherlands) (2001).
[14] Perissin, D., Rocca, F., "High-accuracy urban DEM using permanent scatterers," IEEE TGARS 44(11), 3338–3347 (2006).